Transtension in the Levant Basin: Challenging the Syrian Arc model

Amir Joffe [1*], Rebecca E. Bell[1], Josh Steinberg[2], Christopher A-L. Jackson[1,3], Yizhaq Makovsky[4], Omri Shitrit[5]

1. Landscapes and Basins Research Group (LBRG), Department of Earth Science and Engineering, Imperial College London, South Kensington Campus, SW7 2BP, UK
2.
3. WSP UK Ltd, Manchester, M15 4GU, UK
4. The Dr. Moses Strauss Department of Marine Geoscience and Hatter Department of Marine Technologies, Charney School of Marine Sciences, University of Haifa, 3103301 Haifa, Israel
5. NewMed Energy LP, 19 Abba Eban Boulevard, Herzelia, Israel

1. ABSTRACT

Late Cretaceous intra-plate shortening, and inversion of the Permian to Jurassic rift system, resulted in the ~1000 km-long, S-shaped Syrian Arc Fold Belt which dominates the Levant regional topography through Egypt, Israel, Lebanon, and Syria. Subsequent Miocene folding along the same trends of the Late Cretaceous fold belt, was likely associated with the collision of Arabia and Eurasia. The kinematic model detailing how the Miocene collision initiated the observed inversion is currently unclear yet is essential to our understanding of the geological development of this tectonically complex region. We here present a borehole-constrained seismic-stratigraphic interpretation of 3D seismic reflection data from the Levant Basin that provides unparalleled imaging of these Oligocene-Miocene folds. We show that one of the structures, the NE-SW trending Tamar Anticline, formed during the Burdigalian (lower-Miocene) with no indication of a precursor phase of Late Cretaceous inversion, as previously suggested. We show how the Tamar Anticline was formed concurrent to movement on adjacent strike-slip faults and to the dissection of the anticline by NW-SE-striking normal faults. Simultaneous NW-SE-directed shortening and NE-SW-extension, related to motion along ~E-W strike-slip faults suggests the Tamar Anticline and similar structures developed during the Miocene folding phase formed due to transtension, driven by the opening of the Red-Sea. This new geodynamic model highlights that Late Cretaceous and Miocene folding associated with the Syrian Arc Fold Belt may be geometrically comparable, but stem from different geodynamic regimes.

2. INTRODUCTION

The ~1000 km-long S-shaped fold-belt of the Syrian Arc crosses through Egypt, Israel, Lebanon and Syria (sensu Krenkel, 1924; Figure 1). The folds reflect an inversion-related folding that occurred in two main pulses, termed Syrian Arc I and Syrian Arc II, above pre-existing, late Palaeozoic-early Mesozoic, rift-related normal faults (Walley, 1998). Syrian Arc I occurred during the Late Cretaceous as part of the closure of the Neotethys and the collision of African-Arabian and Eurasian plates (Walley, 1998; Gardosh and Druckman, 2006). This Late Cretaceous compression was part of global plate reorganisation that was responsible for counterclockwise rotation and northward drift of the African-Arabian plate, resulting in an increased rate of convergence with the Eurasian Plate (Guiraud and Bosworth, 1997).

While the kinematic evolution of Syrian Arc I is fairly well understood, that of Syrian Arc II is presently poorly constrained, despite significant offshore hydrocarbon discoveries in associated structures (e.g., Tamar, Leviathan, and Aphrodite fields; Figure 1), and academic interest in the geodynamic significance of the Levant Basin's Miocene folds. For example, Gardosh et al. (2008) speculated that folding initiated in the Middle Miocene, whereas previously proposed ages range from Late Oligocene to Early Miocene (Walley, 1998; Eyal and Reches, 1983), or even continuous folding since the Late Cretaceous into the Pliocene, implying Syrian Arc I and the Miocene folding event cannot be differentiated (Sagy et al. 2018). Despite kinematic ambiguity, most authors agree that the Miocene folding event is related to the formation of Mount Lebanon, and the Bitlis-Suture zone between the Arabia and Eurasian plate, hence likely representing an intra-plate strain signal (Walley, 2011). Yet, how this intra-plate strain shaped the spatial and temporal folds kinematics remain unexplained. Furthermore, significant tectonic events around the Levant, such as the opening of the Red-Sea and the northward propagation of the Dead-Sea Transform, should be integrated in the model.

Unlike those associated with the older event, Miocene folds are located exclusively offshore (Gardosh et al. 2008; Sagy et al., 2018) and seem to have genetic association with normal and strike-slip faults, rather than reverse faults above reactivated rift-related normal faults (Moustafa, 2013; Joffe et al., 2022). Most studies analyse the cross-sectional geometry and kinematics of the folds using 2D seismic reflection data (Gardosh et al., 2008; Sagy et al., 2018) or use 3D seismic reflection data to focus on a single structure (Needham et al., 2017; Goulitis et al., 2019; Joffe et al., 2022). However, a detailed three-dimensional examination using multiple 3D seismic surveys has not been done yet. Such examination would allow to observe the evolution of the structures and their relationship to the regional basin tectonics. Here we use multiple 3D seismic reflection surveys (Figure 1A) to generate thickness maps of age-constrained, Oligocene-Miocene sedimentary sequences and determine folding kinematics in the Levant Basin. We show the mechanisms and likely tectonic drivers for the Miocene (Syrian Arc II) and Cretaceous (Syrian Arc I) folding event.

3. DATA AND METHODOLOGY

Our dataset consists of two 2D and seven 3D, high-quality, pre-stack depth-migrated (PSDM) seismic reflection datasets, covering an area of 9,900 km^2 in the deep-water of the Southern Levant Basin, offshore Israel (Figure 1A). In all surveys, an increase in acoustic impedance with depth generates a positive event (black on seismic profiles), whereas a decrease generates a negative event (white). Seismic intepretation of age-constrained horizons was based on the framework presented by Torfstein and Steinberg (2020) and Joffe et al. (2022) (Figure 1B). The ages of deeper reflections (i.e., sub-Eocene) were constrained using data presented by Steinberg et al. (2018) (Figure 1B). Pre-Upper Jurassic structural highs, where no Oligocene-Miocene depositional occurred, are left unshaded in Figure 1B.

To determine the timing of faulting and folding, we use two techniques. For the folds, we use the approach of Jackson et al. (2013), whereby sediment thickness maps (isopach) indicate intervals of across-fold thinning and therefore, periods of shortening-driven anticline growth (syn-tectonic). For the faults, we follow Jackson et al. (2017), who also use thickness maps and Expansion Index analysis to identify intervals of across-fault thickening that record periods of extension-driven normal fault nucleation and growth (see Expansion Index analysis of 326 faults in Material 1).

4. RESULTS

Thickness maps of the main seismic horizons are presented in Figure 2. These show that Eocene strata (Orange in Figure 1B) are mostly isopachous including across the Tamar Anticline (Figure 2A); the only exception is the Leviathan High, where Eocene thinning is observed, likely due to an underlying Cretaceous high (Steinberg et al., 2018). The overlying Rupelian – Early Burdigalian (33.9 – 17.5 Ma) unit (yellow in Figure 1B) is also isopachous throughout (Figure 2B). In contrast, Upper Burdigalian strata (17.5 – 15 Ma, red in Figure 1B) display significant thickness changes in relation to four different structural elements (Figure 2C):

(1) NW-SE striking, relatively low-displacement, layer-bound normal faults, which are wide-spread across the Levant Basin ("piano-key" faults of Ghalayini et al., 2017; Joffe et al., 2022). Thickness changes in Figure 2C, alongside faults kinematic indicators (Expansion Index and EI and T-z plots; Supplementary Material 1) reveal across-fault thickening of Upper Burdigalian strata, indicating these structures were active during the Late Burdigalian (Joffe et al., 2022); (2) WSW-ENE-striking, basement-involved strike-slip faults (LTK and LTa faults of Joffe et al. 2024), which splay upward to define a negative flower structure (Figure 2C III&IV); (3) NE-SW trending folds, including the eastern flank of the Leviathan High, as well as the Tamar Anticline (~30 km long, ~12 km wide, ~300 m high) (Figure 2C III & IV). Whereas the first is superimposed on the deeper, underlying, basement-involved horst of the Leviathan High, the latter is isolated, being bound by the two strike-slip faults defining its

northern and southern edges (Figure 2); and (4) a SSE-NNW-striking lineament defining the western margin of the Leviathan High.

Overlying, younger strata (15- 5.3 Ma) are thinning above the anticlines but not the normal or strike-slip faults (Joffe et al., 2022; Supplementary material 2&3). This is true for both the Serravallian -Langhian unit (grey in Figure 1B) and the Tortonian unit (light-yellow in Figure 1B).

5. DISCUSSION

Our kinematic analysis shows that the NW-SE-striking normal faults, the NE-SW trending anticlines, the WSW-ENE-striking strike-slip faults, and the SSE-NNW lineament that bound the Leviathan High from the south, all nucleated during the Late Burdigalian. Our thickness maps also show that a significant structural hiatus occurred throughout the Levant between the Rupelian and Early Burdigalian, indicating that folding was not continuous from the Late Cretaceous to present, as previously suggested (e.g., Sagy et al., 2018). Based on these observations, and the broader plate tectonic settings of the study area during the Miocene, we suggest that transtension-related folding provides the most robust kinematic model for the coeval development of fault systems and folds (Figure 3; Sanderson and Marchini, 1984; Venkat-Ramani & Tikoff, 2002; Fossen et al., 2013; Kristensen et al., 2018).

In this model, the additional oblique pure shear extension between two strike-slip faults is accommodated by normal faulting and is balanced by perpendicular folding (Sanderson and Marchini, 1984; Venkat-Ramani & Tikoff, 2002; Fossen et al., 2013; Nabavi et al., 2018; Kristensen et al., 2018) (Figure 3B). These kinematics are exemplified by the Tamar Anticline, in which two strike-slip faults (LTK and LTa) bound the anticline. In response to transtension, the NW-SE piano-key normal faults strike orthogonally to concurrent NE-SE anticline folding (Figure 3C). These observations are consistent with those of Libby et al. (2017), who proposed a similar kinematic relationship between the piano-key faults offshore Lebanon and the contemporaneous, fault-perpendicular folds (Figure 3A). Similar to the Tamar Anticline, the Miocene folds offshore Lebanon are not underlain by compressional anticlines which reactivated (i.e., inverted) normal faults, indicating that they too did not form in response to Cretaceous compression.

The piano-key faults in the southern Levant Basin became inactive by the end of the Langhian (~13 Ma), whereas those in the northern Levant Basin offset the base of the Messinian Evaporites, suggesting they were active until later (i.e., until at least ~5.3 Ma). We suggest this diachroneity records northward propagation of plate boundary deformation, associated with the Dead-Sea Transform which nucleated at its southern tip in the Gulf of Aqaba at ~18 Ma (Early Burdigalian) and propagated northward, reaching the Lebanese restraining bend at ~14 Ma (Late Burdigalian – Langhian) (Nuriel et al., 2017; Oren et al., 2020; 2023).

Similar spatio-temporal relationships between strike-slip faulting, folding and fold-perpendicular normal faulting are observed onshore Sinai (Moustafa, 2013) and offshore Lebanon (Libby et al., 2017). This suggests that rather than reflecting the somewhat poorly constrained, Bitlis-Suture zone-related, far-field, stress field advocated by Wally (1998), regional transtension may explain broadly synchronous, Miocene faulting and folding across the entire Levant area. We suggest the source for this transtension was the Burdigalian opening of the Red-Sea and the related counterclockwise rotation of the Arabian plate (Boone et al., 2021; Sembroni et al., 2024 and references therein), which affected the entire Eastern Mediterranean, including the Levant Basin. More specifically, similar to the Arabian Plate, counterclockwise rotation was also occurring in the Levant Basin with the stagnant Eratosthenes Seamount, alongside northward movement of the eastern Levant and onshore regions, resulted in the activation of the WSW-ENEs-striking strike-slip faults, and therefore transtensional related folding and faulting.

6. CONCLUSION

We show here that despite being geometrically similar, Cretaceous and Miocene folds (previously termed Syrian Arc I & II) formed in response to very different geodynamic regimes. Whereas the Cretaceous folds were initiated in response to a northern orogenic-related compression, related to the collision of Arabia and Eurasia, the Miocene folds were initiated in response to an overall transtensional stress regime that originated due to rift-related opening of the Red Sea and counterclockwise rotation of the Levant Basin and surrounding regions. We also show that folding in the deep Levant Basin was pulsed rather than continuous from the Late Cretaceous to present, whereas a significant folding hiatus took place during the Rupelian – Early Burdigalian (33.9 – 17.5 Ma). We present the complicated array of coeval folding, fold-perpendicular normal faulting, strike-slip faulting associated with opening of the Red-Sea, counterclockwise rotation of Arabia, nucleation of the Dead-Sea transform, and the northward propagation of the plate-driven stress regime. This reorganisation was manifested in the Levant Basin by the initiation of strike-slip faulting, which created a transtensional strain field between them. Our work recalls that not all folds record inversion and causal co-axial compression, but instead record transtension-related faulting.

ACKNOELEDMENTS

We would like to thank Ratio Energies for their financial support of Amir Joffe's PhD and for providing the 2D surveys, and the Leviathan, Royee, Sara-Myra-Arie 3D seismic reflection data. We extend our thanks to NewMed Energy and Chevron for approving access to the Leviathan 3D survey. We would like to extend our thank to Isramco for access to the Tamar 3D seismic reflection survey. Lastly, we would like to thank the Petroleum Commissioner of Israel for providing access to the NBL 3D survey. We would like to thank SLB for their academic licenses to Imperial College. Kul Karcz and Adar Glazer are thanked for fruitful discussion and support during the preparations of this manuscript.

REFERENCES CITED

Boone, S. C., Balestrieri, M. L., & Kohn, B., 2021, Thermo-tectonic imaging of the Gulf of Aden-Red Sea rift systems and Afro-Arabian hinterland, Earth-Science Reviews, *222*, 103824. https://doi.org/10.1016/j.earscirev.2021.103824

Eyal, Y., & Reches, Z. E., 1983, Tectonic analysis of the Dead Sea Rift Region since the Late-Cretaceous based on mesostructures. Tectonics, 2(2), 167-185. https://doi.org/10.1029/TC002i002p00167

Fossen, H., Teyssier, C., & Whitney, D. L., 2013, Transtensional folding. Journal of Structural Geology, 56, 89-102. https://doi.org/10.1016/j.jsg.2013.09.004

Gardosh, M. A., & Druckman, Y. ,2006, Seismic stratigraphy, structure and tectonic evolution of the Levantine Basin, offshore Israel. Geological Society, London, Special Publications, 260(1), 201. https://doi.org/10.1144/GSL.SP.2006.260.01.09

Gardosh, M., Druckman, Y., Buchbinder, B., & Rybakov, M., 2008, The Levant Basin Offshore Israel: Stratigraphy, Structure, Tectonic Evolution and Implications for Hydrocarbon Exploration - revised edition. Geological Survey of Israel report GSI/4/2008 (Issue April). Geological Survey of Israel.

Ghalayini, R., C. Homberg, J. M. Daniel, and F. H. Nader, 2017, Growth of layer-bound normal faults under a regional anisotropic stress field: Geological Society, London, Special Publications, v. 439, no. 1, p. 57 LP – 78, doi:10.1144/SP439.1

Gouliotis, L., 2019, Tectonic Structure of the Karish Gas Field, Offshore Israel Tectonics and Hydrogeology of Sterea Hellas View project Researches on the geology of Greece View project: Search and Discovery, no. 30638, doi:10.1306/30638Gouliotis2019.

Guiraud, R., & Bosworth, W., 1997, Senonian basin inversion and rejuvenation of rifting in Africa and Arabia: synthesis and implications to plate-scale tectonics. Tectonophysics, 282(1-4), 39-82. https://doi.org/10.1016/S0040-1951(97)00212-6

Jackson, C. A. L., and A. Rotevatn, 2013, 3D seismic analysis of the structure and evolution of a salt-influenced normal fault zone: A test of competing fault growth models: Journal of Structural Geology, v. 54, p. 215–234, doi:10.1016/j.jsg.2013.06.012.

Jackson, C. L., Chua, S. T., Bell, R. E., & Magee, C., 2013, Structural style and early stage growth of inversion structures: 3D seismic insights from the Egersund Basin, offshore Norway. Journal of Structural Geology, 46, 167-185. https://doi.org/10.1016/j.jsg.2012.09.005

Jackson, C. A. L., R. E. Bell, A. Rotevatn, and A. B. M. Tvedt, 2017, Techniques to determine the kinematics of synsedimentary normal faults and implications for fault growth models: Geological Society Special Publication, v. 439, no. 1, p. 187–217, doi:10.1144/SP439.22.

Joffe, A., Jackson, C. A. L., Steinberg, J., Bell, R. E., & Makovsky, Y., 2023, Origin and kinematics of a basin-scale, non-polygonal, layer-bound normal fault system in the Levant Basin, eastern Mediterranean. Basin Research, 35(2), 662-691. https://doi.org/10.1111/bre.12729

Joffe, A., Bell, R. E.., Steinberg, J, Jackson, C. A. L., & Makovsky, Y., 2024, Oligocene-Miocene Tectono-Stratigraphic Development of the Southern Levant Basin, Eastern Mediterranean. EarthArxiv, https://doi.org/10.31223/X59M6P

Krenkel, E., 1924, Der Syrische Bogen. Zentralblatt Mineralogie, 9(10), 274–281.

Kristensen, T. B., Rotevatn, A., Marvik, M., Henstra, G. A., Gawthorpe, R. L., & Ravnås, R., 2018, Structural evolution of sheared margin basins: The role of strain partitioning. Sørvestsnaget Basin, Norwegian Barents Sea. Basin Research, 30(2), 279-301. https://doi.org/10.1111/bre.12253

Libby, S. A., 2017, Implications of seismic data for the structural evolution and numerical modelling of the Eastern Mediterranean Basin [PhD dissertation]: Edinburgh, Harriot-Watt University, 387. http://hdl.handle.net/10399/3440

Moustafa, A. R., 2013, Fold-related faults in the Syrian Arc belt of northern Egypt. Marine and Petroleum Geology, 48, 441-454. https://doi.org/10.1016/j.marpetgeo.2013.08.007

Nabavi, S. T., Alavi, S. A., & Maerten, F., 2018, 2D finite-element elastic models of transtensional pull-apart basins. Comptes Rendus Geoscience, 350(5), 222-230. https://doi.org/10.1016/j.crte.2018.06.001

Needham, D. L., H. S. Pettingill, C. J. Christensen, J. Ffrench, and Z. K. Karcz, 2017, The Tamar giant gas field: Opening the Subsalt Miocene gas play in the Levant Basin, in AAPG Memoir: American Association of Petroleum Geologists, p. 221–256, doi:10.1306/13572009M1133688.

Nuriel, P., Weinberger, R., Kylander-Clark, A. R. C., Hacker, B. R., & Craddock, J. P., 2017, The onset of the Dead Sea transform based on calcite age-strain analyses. Geology, 45(7), 587–590. https://doi.org/10.1130/G38903.1

Oren, O., Nuriel, P., Kylander-Clark, A. R. C., & Haviv, I., 2020, Evolution and propagation of an active plate boundary: U-Pb ages of fault-related calcite from the Dead Sea Transform. Tectonics, 39, e2019TC005888. https://doi.org/10.1029/2019TC005888

Oren, O., Nuriel, P., Kylander-Clark, A. R. C., & Haviv, I., 2023, Deciphering the Africa-Arabia: Insights from U-Pb dating along the Carmel-Gilboa fault system and its triple junction with the Dead Sea transform. Earth and Planetary Science Letters, 611, 118152. https://doi.org/10.1016/j.epsl.2023.118152

Sagy, Y., Gvirtzman, Z., & Reshef, M., 2018, 80 my of folding migration: New perspective on the Syrian arc from Levant Basin analysis. Geology, 46(2), 175-178. https://doi.org/10.1130/G39654.1

Sanderson, D. J., & Marchini, W. R. D., 1984, Transpression. Journal of structural Geology, 6(5), 449-458. https://doi.org/10.1016/0191-8141(84)90058-0

Sembroni, A., Faccenna, C., Becker, T. W., & Molin, P., 2024, The uplift of the East Africa-Arabia swell. Earth-Science Reviews, 104901. https://doi.org/10.1016/j.earscirev.2024.104901

Steinberg, J., Roberts, A. M., Kusznir, N. J., Schafer, K., & Karcz, Z., 2018, Crustal structure and post-rift evolution of the Levant Basin. Marine and Petroleum Geology, 96, 522-543.

Torfstein, A., & Steinberg, J., 2020, The Oligo–Miocene closure of the Tethys Ocean and evolution of the proto-Mediterranean Sea. Scientific Reports, 10(1), 13817.

Venkat-Ramani, M., & Tikoff, B., 2002, Physical models of transtensional folding. Geology, 30(6), 523-526. https://doi.org/10.1130/0091-7613(2002)030<0523:PMOTF>2.0.CO;2

Walley, C. D., 1998, Some outstanding issues in the geology of Lebanon and their importance in the tectonic evolution of the Levantine region. Tectonophysics, 298(1-3), 37-62. https://doi.org/10.1016/S0040-1951(98)00177-2

Walley, C. D., 2001, The Lebanon passive margin and the evolution of the Levantine Neo-Tethys. Peri-Tethys Memoir, 6, 407-439.

FIGURE CAPTIONS

Figure 1: (A) Location map of the study area and the main structural elements. Insert shows the outline of the dataset used; the main structural elements highlighted in Figure 1B. Figure 1B location is highlighted in Yellow. The bathymetric metadata and Digital Terrain Model data products have been derived from the EMODnet Bathymetry portal – http//www.emodnet-bathymetry.eu. (B) Cross section through the main structural highs in the basin.

Figure 2: (A) Thickness map of the Eocene – Senonian unit, highlighting the isopachous deposition across the Tamar anticline. (B) Thickness map of the Oligocene – Early Miocene indicating isopachous deposition across the deep basin. Highlighted is the isopachous deposition in Tamar. (C) Thickness map of the Late Burdigalian showing distinct thickness changes across the basin. White numbers indicate major structural elements highlighted in the text (including LTK and LTa dextral wrench systems). Yellow numbers indicate the location of the cross-sections highlighted in D. (D) cross-sections highlighting the strike-slip negative flower structure, and the Upper Burdigalian growth strata associated with the faulting and folding.

Figure 3: Conceptual model explaining the transtensional related folding model in the Levant Basin. (A) simplified map showing the main strike-slip, anticlines and perpendicular normal faulting. Also highlighted is the strain ellipse that fits our observations. (B) theoretical model for transtension (modified from Sanderson and Marchini, 1984). (C) zoomed in simplified map of the structural elements around Tamar and Leviathan indicating the similarities of the model presented in B.

Figures

Figure 1

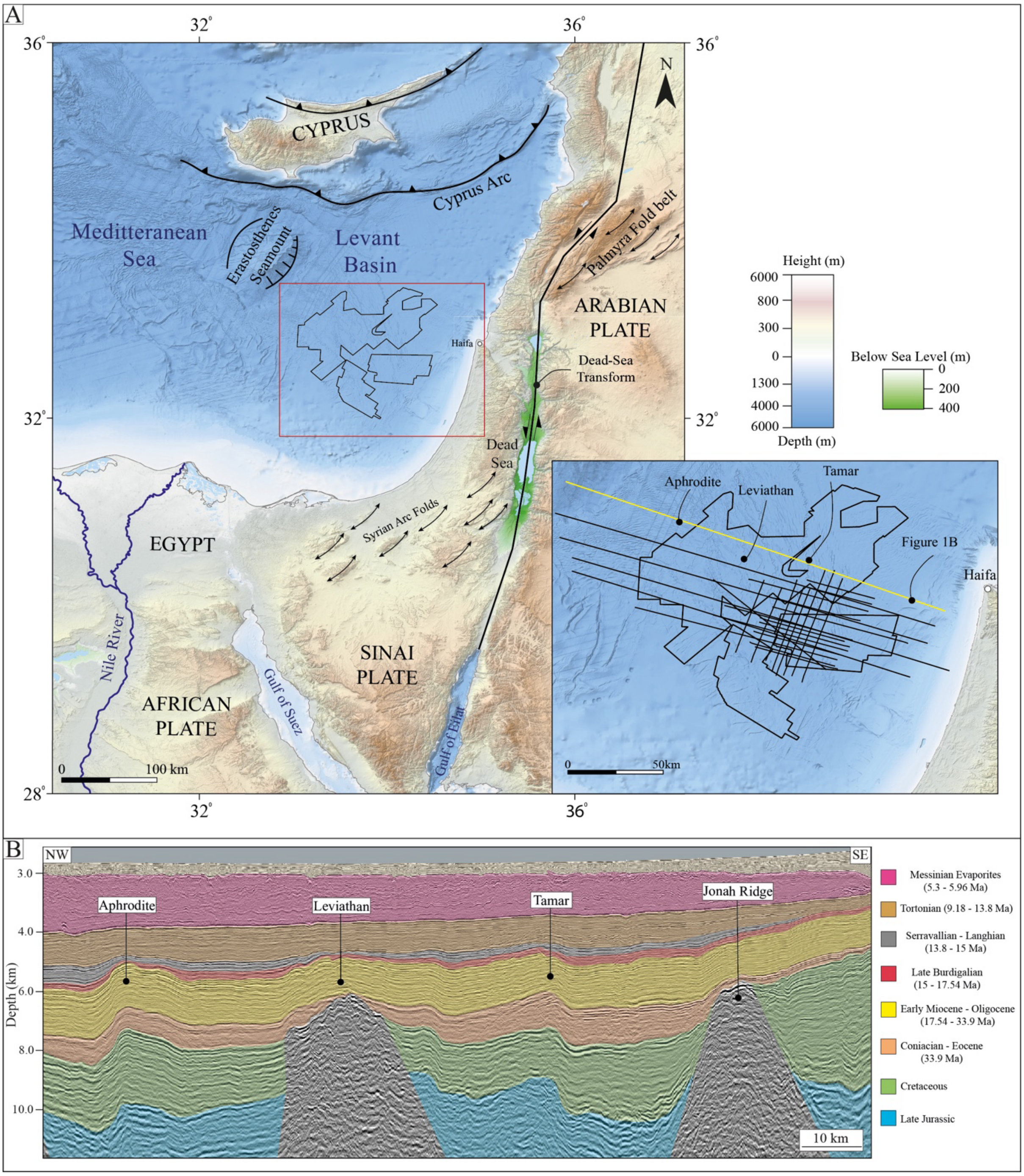

308 Figure 2

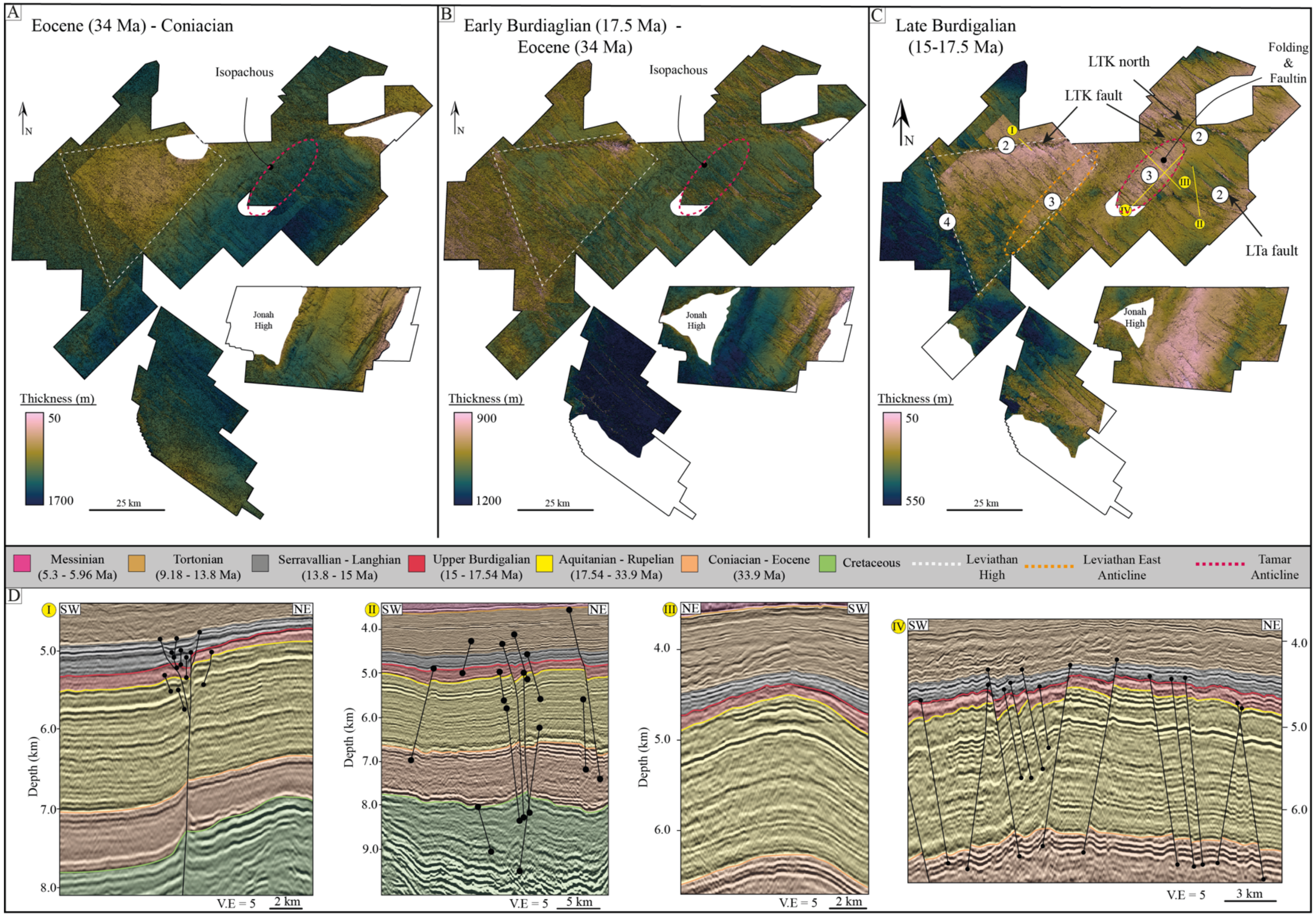

309

310

Figure 3

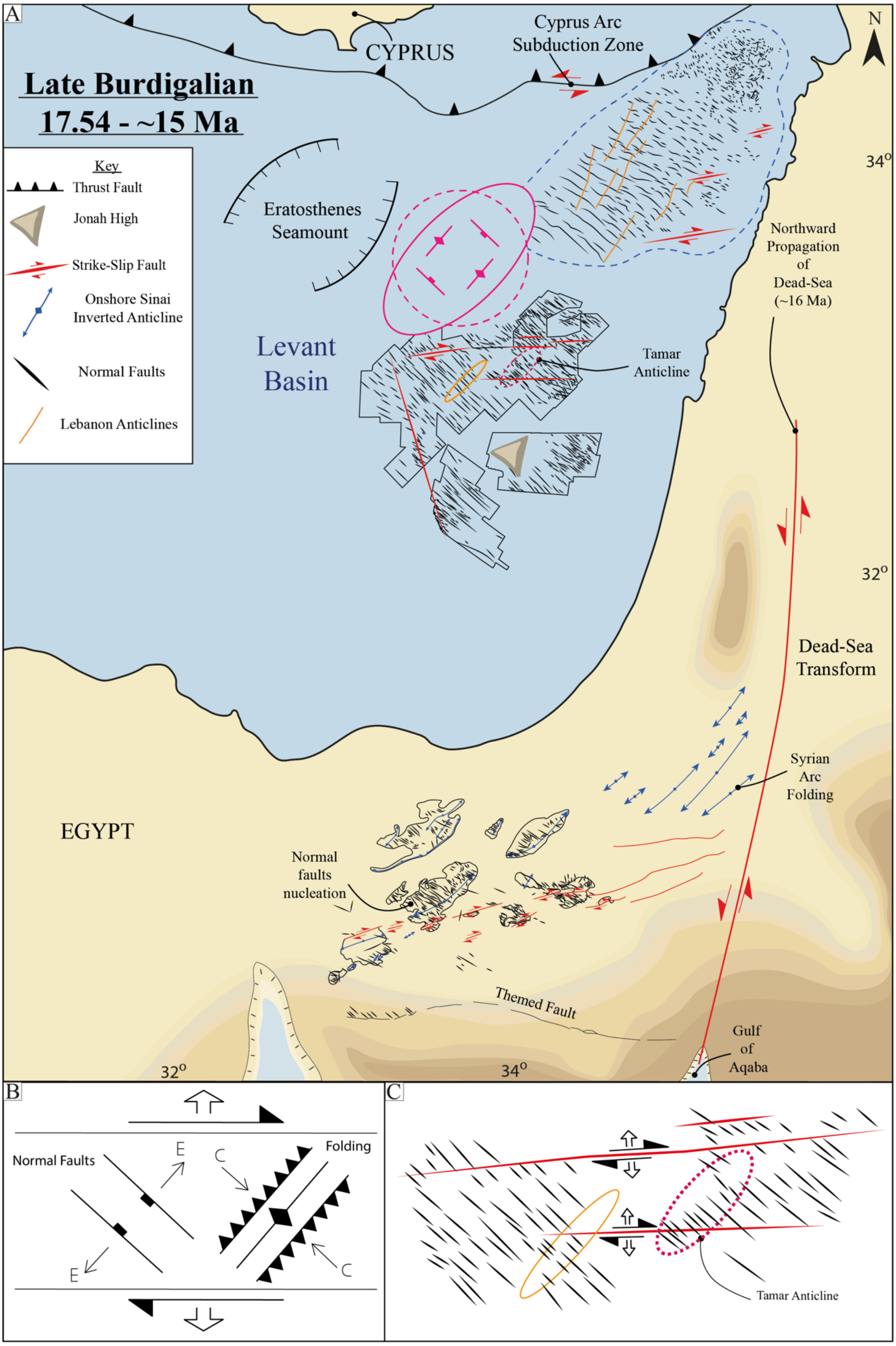
A
Late Burdigalian
17.54 - ~15 Ma
CYPRUS
Cyprus Arc
Subduction Zone
N
34°
Key
Thrust Fault
Jonah High
Strike-Slip Fault
Onshore Sinai
Inverted Anticline
Normal Faults
Lebanon Anticlines
Eratosthenes
Seamount
Levant
Basin
Tamar
Anticline
Northward
Propagation
of
Dead-Sea
(~16 Ma)
32°
Dead-Sea
Transform
Syrian
Arc
Folding
EGYPT
Normal
faults
nucleation
Themed Fault
Gulf
of
Aqaba
32°
34°
B
Normal Faults
E
C
Folding
E
C
C
Tamar Anticline

Supplementary Material

<u>Supplementary Material 1 – Fault Kinematic Analysis</u>

326 T-z and Expansion index (EI>1) plots help identify growth strata as a sign for fault nucleation (Jackson et al., 2017).

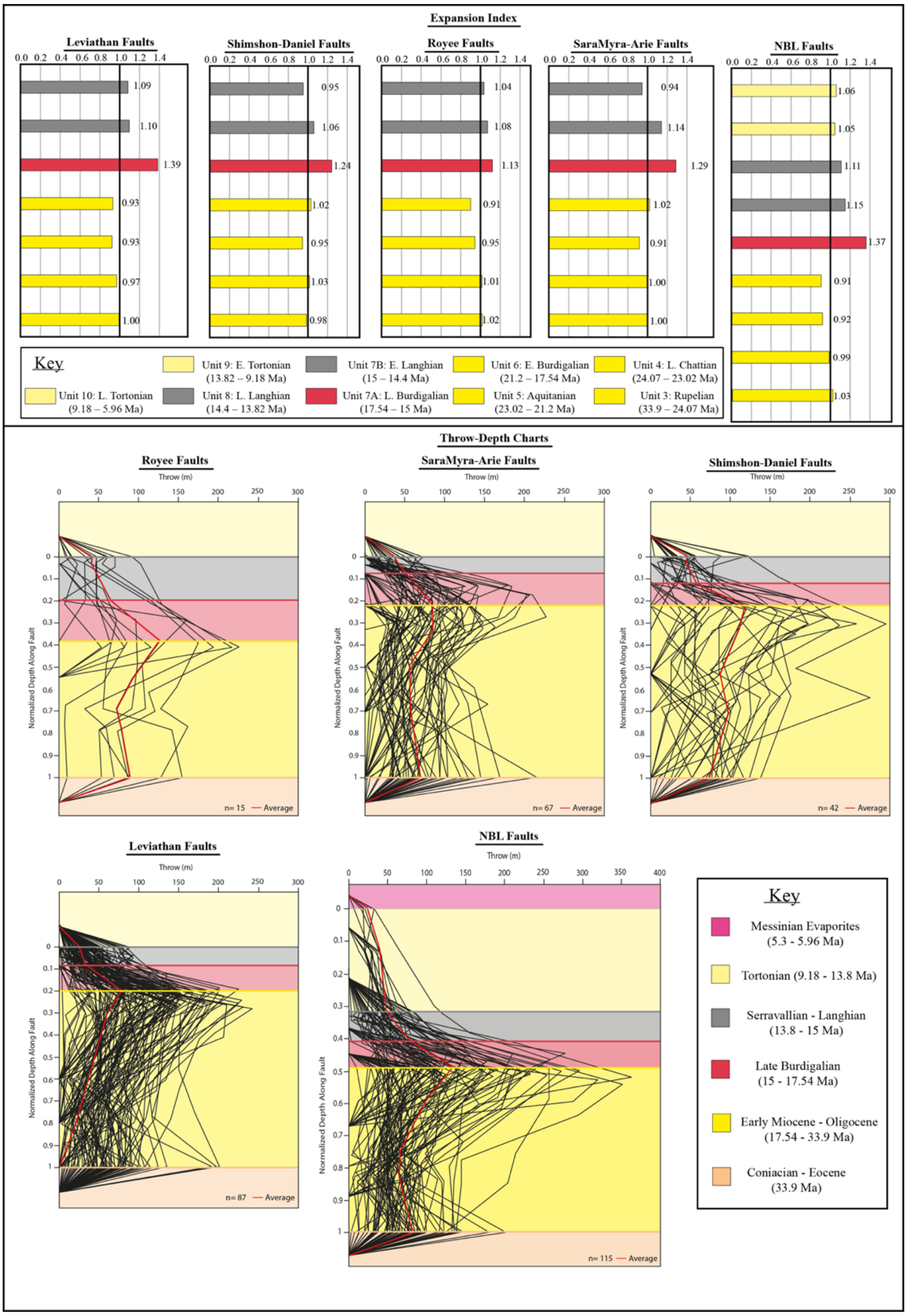

Supplementary Material 2 – Serravallian – Langhian Thickness map

Thinning is only observed above the anticlines, with no significant changes associated with the normal or strike-slip faults.

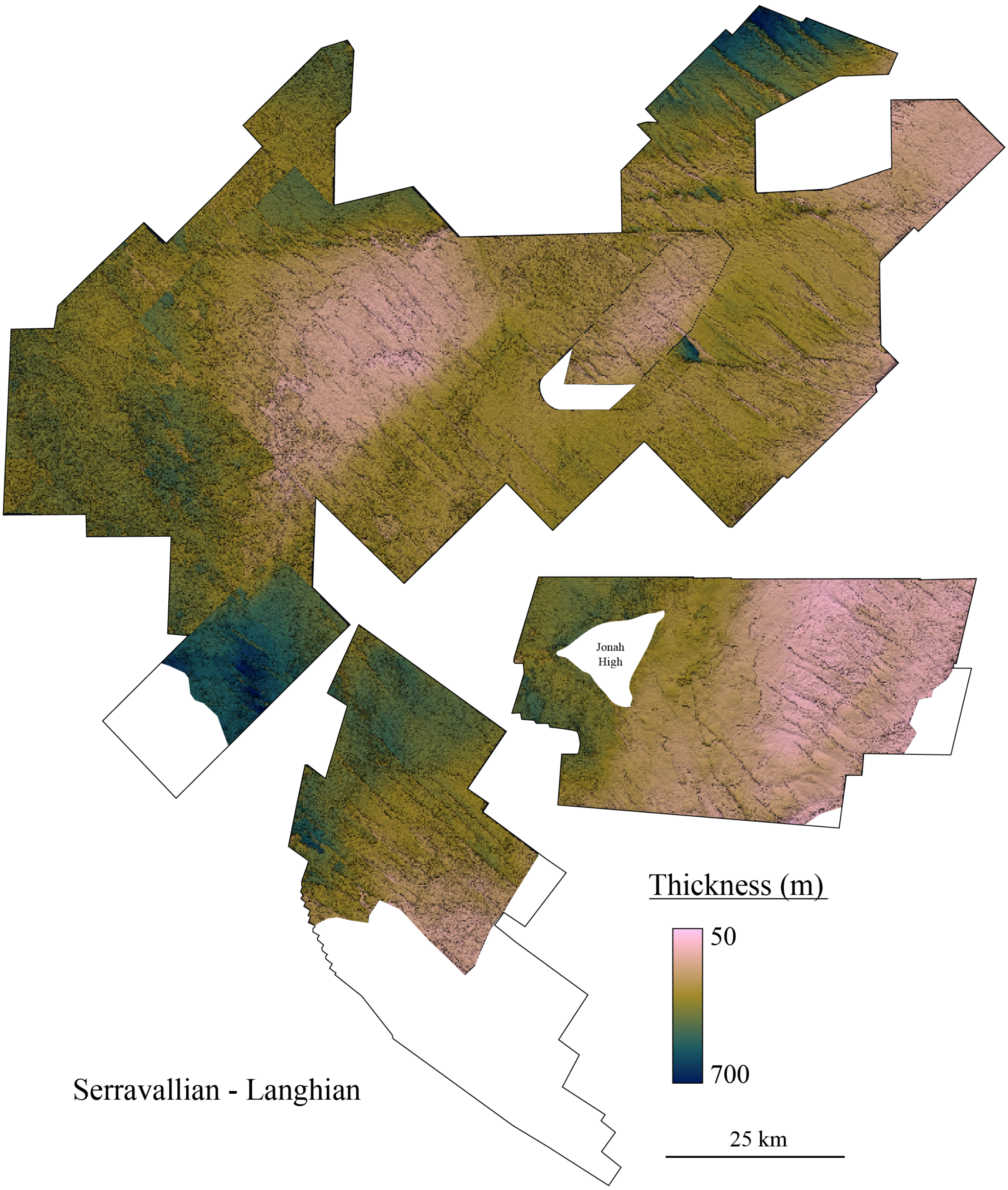

Supplementary Material 3 – Tortonian Thickness Map

Thinning is only observed above the anticlines, with no significant changes associated with the normal or strike-slip faults.